Indian Journal of Chemistry
Vol. 64, July 2025, pp. 730-745
DOI: 10.56042/ijc.v64i7.16642

Repurposing FDA-approved antimalarial drugs: Mefloquine as a promising multi-targeted therapeutic for non-small cell lung cancer

Vicky Lone[a], Kanak Dayama[a], Pratik Khona[a] & Uma D Kabra*[a,b]

[a] Department of Pharmaceutical Chemistry, Parul Institute of Pharmacy, Parul University, Vadodara 391 760, Gujarat, India

[b] Department of Pharmaceutical Chemistry, Smt. Kishoritai Bhoyar College of Pharmacy, New Kamptee, Nagpur 441 002, Maharashtra, India

E-mail: uma.kabra05@gmail.com

Received 24 January 2025; accepted (revised) 16 June 2025

Lung cancer, particularly non-small cell lung cancer (NSCLC), remains a major global health challenge, accounting for 85% of cases. Despite progress in immunotherapy targeting mutations like EGFR, MET, and RET, issues such as drug resistance, high treatment costs, and limited efficacy persist. Drug repurposing has emerged as a promising strategy to overcome these obstacles. This study investigates the potential of FDA-approved antimalarial drugs as multi-target therapies for NSCLC. Fourteen antimalarial drugs have been screened using molecular docking, leveraging their established safety profiles. Mefloquine (MQ), artesunate, artemether, and quinine show strong binding affinities for EGFR, MET, and RET targets, with MQ exhibiting the most significant interactions. Molecular dynamics (MD) simulations have confirmed MQ's stability and favorable binding to these targets, supported by RMSD, RMSF, and Rg analyses. *In vitro* tests using the Sulforhodamine B (SRB) assay demonstrate a dose-dependent inhibitory effect of MQ on A549 NSCLC cell proliferation, with notable reductions in cell viability at concentrations as low as 10 µM. The findings suggest MQ's potential as a cost-effective therapeutic candidate for NSCLC treatment, either alone or in combination with other therapies. Further research is needed to explore MQ's anticancer mechanisms and optimize its clinical use.

Keywords: Repurposing, Antimalarial, Mefloquine, Docking, Dynamic simulation, Anticancer

Lung cancer ranks as the second most commonly diagnosed cancer worldwide, poses a major health challenge, with a higher incidence in men than women. In 2022, lung cancer was responsible for 2.48 million new diagnoses and 1.8 million deaths globally. This burden is expected to increase, with projections indicating 4.62 million new cases and 3.55 million deaths by 2050[1] . Non-small cell lung cancer (NSCLC) accounts for approximately 85% of lung cancer cases and includes subtypes such as adenocarcinoma, squamous cell carcinoma, and large cell carcinoma. Smoking is the primary risk factor, along with environmental, genetic, and lifestyle factors[2]. Primary treatments like surgery, radiotherapy, and chemotherapy often face challenges such as drug resistance and significant side effects, limiting their effectiveness[3].

NSCLC is driven by genetic alterations like mutations, amplifications, and fusions in genes such as Epidermal Growth Factor Receptor (EGFR), Mesenchymal-Epithelial Transition Factor (MET), and Rearranged during Transfection (RET), which promote tumor growth and progression. These genes encode receptor tyrosine kinases critical for cell signaling and survival[4,5]. EGFR mutations, common in adenocarcinoma, lead to uncontrolled cell proliferation and are effectively targeted by tyrosine kinase inhibitors (TKIs) like gefitinib, erlotinib, and osimertinib[6]. MET amplifications and exon 14 skipping mutations drive tumor growth and metastasis, with inhibitors like crizotinib and capmatinib blocking these pathways[7]. RET fusions and mutations, though less frequent, are oncogenic drivers addressed by inhibitors like selpercatinib and pralsetinib[8]. Advanced targeted therapies and immunotherapies have shown significant success in managing NSCLC by disrupting aberrant signaling pathways[9]. Despite advancements in NSCLC treatments, limitations such as severe side effects, drug resistance, limited effectiveness, and high costs highlight the need for continued research to develop safer and more effective therapies.

Drug repurposing, or repositioning, utilizes approved drugs developed for one condition to treat other diseases. This approach takes advantage of

established safety profiles and mechanisms of action, offering a faster and more cost-effective alternative to traditional drug discovery[10]. Notable examples include thalidomide, metformin, and aspirin, initially used for sedation, diabetes, and inflammation, now successfully repurposed for various cancers[11,12]. Similarly, chemotherapeutic agents like cisplatin, originally approved for testicular and ovarian cancers, are being explored for treating lung, bladder, and head and neck cancers[13].

The molecular complexity of NSCLC highlights the need for therapies targeting multiple pathways to overcome resistance. Multi-target drugs have the ability to improve therapeutic effectiveness and reduce adverse effects, addressing the limitations of conventional treatments.

In this regard, antimalarial drugs have shown potential as effective options for cancer treatment due to their known safety profiles and cost-effectiveness[14,15]. Drugs like chloroquine, an autophagy inhibitor, and artemisinin, a ROS generator, have shown encouraging results in preclinical and clinical studies[16,17]. Their repurposing leverages existing data to expedite the development of new treatment options, with ongoing research essential to fully realize their potential in oncology.

This study explores the potential of FDA-approved antimalarial drugs as multi-targeted therapeutics for NSCLC by examining their interactions with key molecular targets. Integrating computational methods like molecular docking and dynamic simulations with experimental validation, the research aims to evaluate their efficacy and mechanisms of action.

Materials and Methods

Data collection and preparation

In this study, 14 FDA-approved antimalarial drugs were obtained from the DrugBank database (www.drugbank.ca). The 2D structures of these drugs were drawn using ChemDraw Pro 21.0 software and subsequently converted into 3D structures with Chem3D 21.0 software, then saved in pdb format. Energy minimization was carried out utilizing the CHARMm force field in Discovery Studio Client (DSC) version 4.1.

Molecular docking and validation

The three-dimensional X-ray crystal structures of the target proteins EGFR (PDB:1M17, resolution = 2.60 Å), cMET (PDB:4R1Y, resolution = 2.00 Å), and RET (PDB:4CKJ, resolution = 1.65 Å) complexed with 4-anilinoquinazoline inhibitor (erlotinib), pyridazinone derivatives, and adenosine, respectively, were extracted from the Protein Data Bank (PDB) (https://www.rcsb.org/pdb) in .pdb format. The protein structures were imported into BIOVIA Discovery Studio and processed by removing the co-crystal ligand, water molecules, and phosphate ions, and adding polar hydrogens and Kollman charges utilizing AutoDock Tools 4.1.1. The optimized proteins were stored in .pdbqt format and then loaded into Autodock Software for molecular docking analysis[18]. The binding pocket of the target protein was decided using a precomputed grid as mentioned:

For PDB 1M17: X = 22.013690, Y = 0.252828, Z = 52.794034; grid size 35 × 35 × 35 Å.
For PDB 4R1Y: X = 22.581507, Y = 27.876582, Z = 103.241687; grid size 40 × 40 × 40 Å.
For PDB 4CKJ: X = 26.492158, Y = 10.737579, Z = 10.237158; grid size 40 × 40 × 40 Å.

First, the docking procedure was validated by removing the inhibitor from the complex and subsequently redocking it into the active site. The RMSD between the redocked ligand and the co-crystallized ligand was then calculated[19,20] . Following validation, all 14 ligands were prepared and docked using AutoDock Vina and PADRE & PERL IDE for multiple docking. The binding poses were clustered and ranked according to their binding affinities. The docking models obtained were visualized using BIOVIA Discovery Studio software, and the key active site residues involved in the interaction were studied.

Molecular dynamic simulation

A 100 ns molecular dynamics (MD) simulation was performed using the GROMACS 2018.1 software package. The energy minimization of the selected protein-ligand complexes, as well as the standard drugs with the target proteins, was carried out using the GROMOS 54a7 force field. Structural topologies for the ligand complexes were generated using the PRODRG web server. The system was simulated in an SPC water model within a cubic box. To neutralize the system, sodium (Na+) and chloride (Cl-) ions were introduced, replacing water molecules and ensuring proper periodic boundary conditions. The system was equilibrated at a temperature of 300 K and a pressure of 1 atm. The Nose-Hoover thermostat and Martyne-Tobias-Klein barostat were employed to

maintain consistent temperature and pressure during the 100 ns simulation. Key parameters, including RMSD, RMSF, and radius of gyration (Rg), were analyzed based on the MD simulation trajectories[21].

Anticancer evaluation

MQ was obtained from Sigma-Aldrich. The cytotoxicity of the compound was evaluated using the SRB assay[22]. In this assay, the A549 NSCLC cell line was plated into 96-well plates at a density of 5,000 cells per well. After allowing the cells to adhere overnight, they were exposed to varying concentrations of the compound (1–60 μM) for 48 hours. Following the treatment, cold trichloroacetic acid was added to halt the assay. The cells were fixed with trichloroacetic acid for 60 min at 4°C. After discarding the supernatant, the plate was washed five times with water and allowed to air dry. Subsequently, the cells were stained with 0.4% (w/v) SRB in 1% acetic acid for 20 min at room temperature. After five washes with a 1% acetic acid solution, the bound dye was solubilized in 10 mM tris base solution. The optical density was measured at 540 nm, and cell viability was calculated.

Results and Discussion

The main objective of this study is to investigate the potential of antimalarial medications drugs as repurposed therapies for the treatment of NSCLC. For this, we extracted 14 FDA-approved antimalarial drugs from the DrugBank database (www.drugbank.ca) and screened them using docking studies against multiple NSCLC targets EGFR, MET, and RET proteins. Given that these FDA-approved drugs have already been validated through preclinical and clinical trials for patient safety, we bypassed further *in silico* drug-likeness filtering. Based on the binding energy, four drugs artesunate, artemether, mefloquine, and quinine exhibited better/comparable binding energy against all three targets compared to reference drugs. Based on the intermolecular interaction between the selected drugs and binding site residues of EGFR, MET, and RET proteins, we identified one ligand that exhibited the highest binding energy and strongest amino acid interactions with all three target proteins. The top-performing ligand was then subjected to MD simulation and assessed for cytotoxic efficacy against the NSCLC cell line.

Initially, the generated grid for each target protein was validated by removing the co-crystallized ligand and then re-docking it into the protein's binding site to obtain the RMSD valueThe redocking process is represented in Fig. 1. The RMSD values between the co-crystallized ligand and the re-docked ligand were 1.4223 Å (Fig. 1A), 1.279 Å (Fig. 1B), and 0.348 Å (Fig. 1C), respectively. These values indicate a good alignment between the docked pose and the co-crystallized structure, confirming that the docking procedure is reproducible, reliable, and that the generated grid accurately represents the binding site.

Subsequently, all antimalarial drugs were docked using the same validation protocol and grid box settings against the three targets, and the results are presented in Table 1. The binding free energy of the antimalarial drugs ranged from –6.6 to –10.4 kcal/mol across the three targets. For comparison, the binding free energy of the co-crystallized ligand inhibitors for PDB IDs 1M17, 4R1Y, and 4CKJ were –7.3 kcal/mol, –8.7 kcal/mol, and –7.6 kcal/mol, respectively.

In the context of binding energy, most of the drugs demonstrated good binding affinity to EGFR compared to the reference drug erlotinib, with the exceptions being chloroquine, hydroxychloroquine, primaquine, proguanil, and sulfadoxine. On the other hand, only four drugs—artesunate, atovaquone, mefloquine, and quinine—showed comparable or better binding affinity to MET compared to the reference pyridazine derivatives. Similarly, most drugs exhibited a stronger binding affinity to RET compared to the reference drug adenosine, except chloroquine, hydroxychloroquine, primaquine, and sulfadoxine. Importantly, the four drugs—artesunate, atovaquone, mefloquine, and quinine—demonstrated favorable binding energy across all three selected targets. Consequently, these drugs were further examined in detail for their interacting amino acids.

Protein-ligand interactions are central to many biological processes and drug discovery efforts. Understanding the binding affinity, specificity, and stability of these complexes is crucial for developing effective therapeutic agents. This knowledge is vital for designing effective and selective therapeutic agents. The interaction of erlotinib with EGFR, pyridoxine derivatives with MET, and adenosine with RET is depicted in Fig. 2 and the amino acid interactions of the four selected drugs are shown in Table 2.

Based on a detailed analysis of binding energy and amino acid interactions of the selected drugs against all three targets, MQ emerged as the only compound exhibiting superior binding energy and the highest degree of amino acid residue interactions compared to the other drugs. Consequently, MQ was selected for further in-depth investigation.

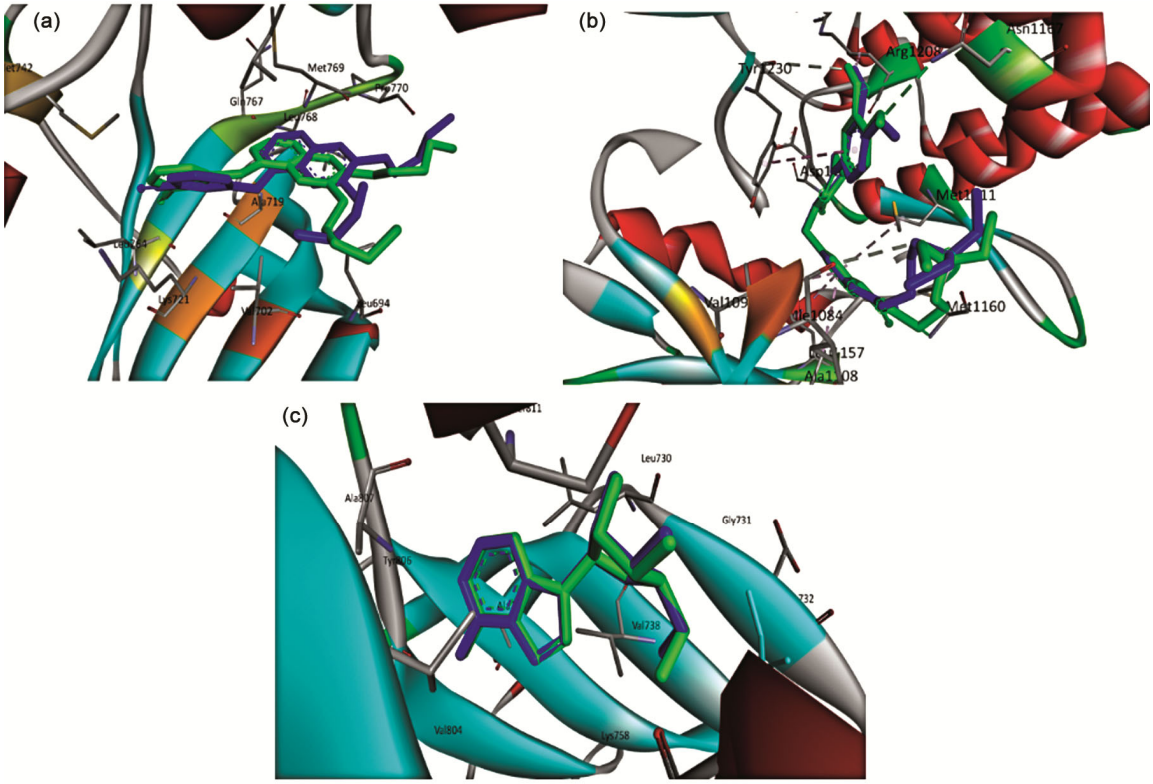

Fig. 1 — Superimposed structures of re-docked ligand (blue) and co-crystallized ligand conformations (green) within the active site of A. EGFR (PDB: 1M17); B. MET (PDB: 4R1Y); and C. RET (PDB: 4CKJ).

Table 1 — Structures and binding energies of the antimalarial drugs against EGFR (PDB 1M17), MET (PDB 4R1Y), and RET (PDB 4CKJ)

S. No.	Drugs	Structure	Binding energy (kcal/mol)		
			EGFR	MET	RET
	Erlotinib	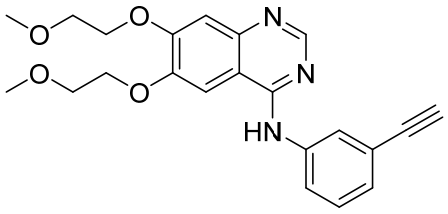	–7.3	–	–
	Pyridazine derivative	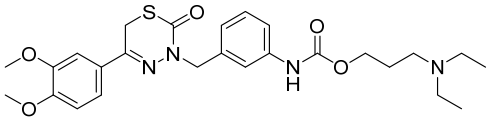	–	–8.7	–
	Adenosine	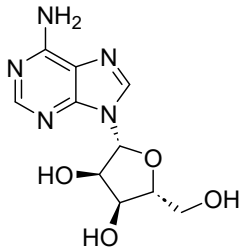	–	–	–7.6

(*Contd.*)

Table 1 — Structures and binding energies of the antimalarial drugs against EGFR (PDB 1M17), MET (PDB 4R1Y), and RET (PDB 4CKJ) (*Contd*.)

S. No.	Drugs	Structure	Binding energy (kcal/mol)		
			EGFR	MET	RET
1	Artemether	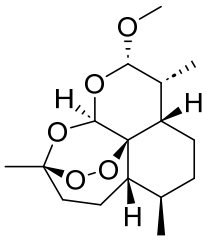	–8.2	–8.1	–8.0
2	Artesunate	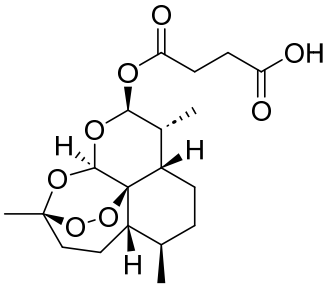	–8.7	–8.7	–8.3
3	Atovaquone	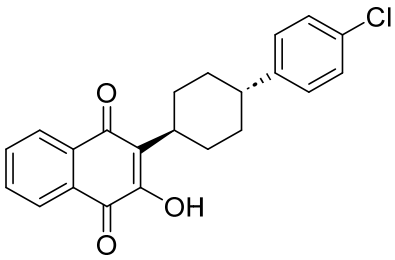	–9.7	–8.7	–10.3
4	Chloroquine	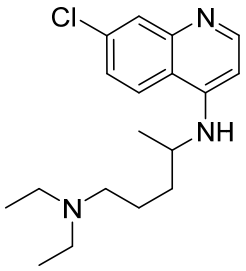	–6.6	–6.8	–7.4
5	Doxycycline	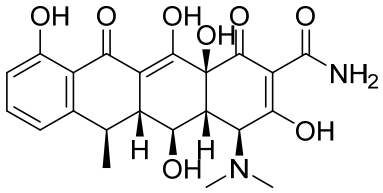	–7.8	–7.3	–7.9
6	Hydroxychloroquine	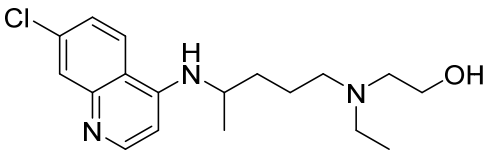	–6.6	–6.8	–7.3

(*Contd*.)

Table 1 — Structures and binding energies of the antimalarial drugs against EGFR (PDB 1M17), MET (PDB 4R1Y), and RET (PDB 4CKJ) (*Contd.*)

S. No.	Drugs	Structure	Binding energy (kcal/mol)		
			EGFR	MET	RET
7	Lumefantrine	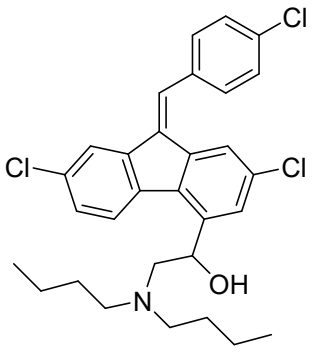	–8.2	–7.4	–8.6
8	Mefloquine	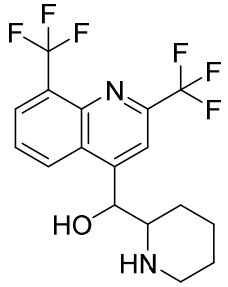	–9.1	–9.3	–10.4
9	Primaquine	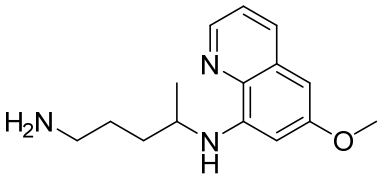	–6.8	–7.2	–7.2
10	Proguanil	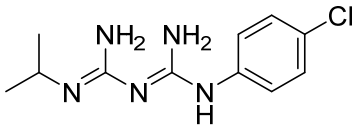	–6.9	–7.3	–7.9
11	Pyrimethamine	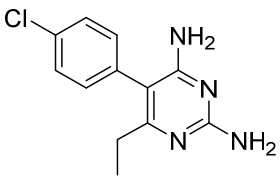	–7.9	–6.9	–7.6
12	Quinine	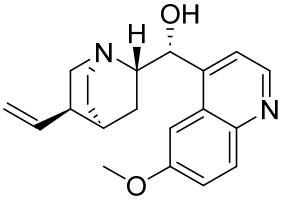	–7.4	–8.7	–8.5

(*Contd.*)

Table 1 — Structures and binding energies of the antimalarial drugs against EGFR (PDB 1M17), MET (PDB 4R1Y), and RET (PDB 4CKJ)

S. No.	Drugs	Structure	Binding energy (kcal/mol)		
			EGFR	MET	RET
13	Sulfadoxine	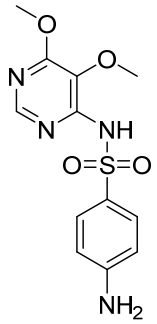	–7.0	–8.1	–7.4
14	Tafenoquine	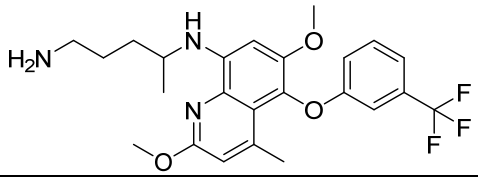	–7.7	–7.8	–9.1

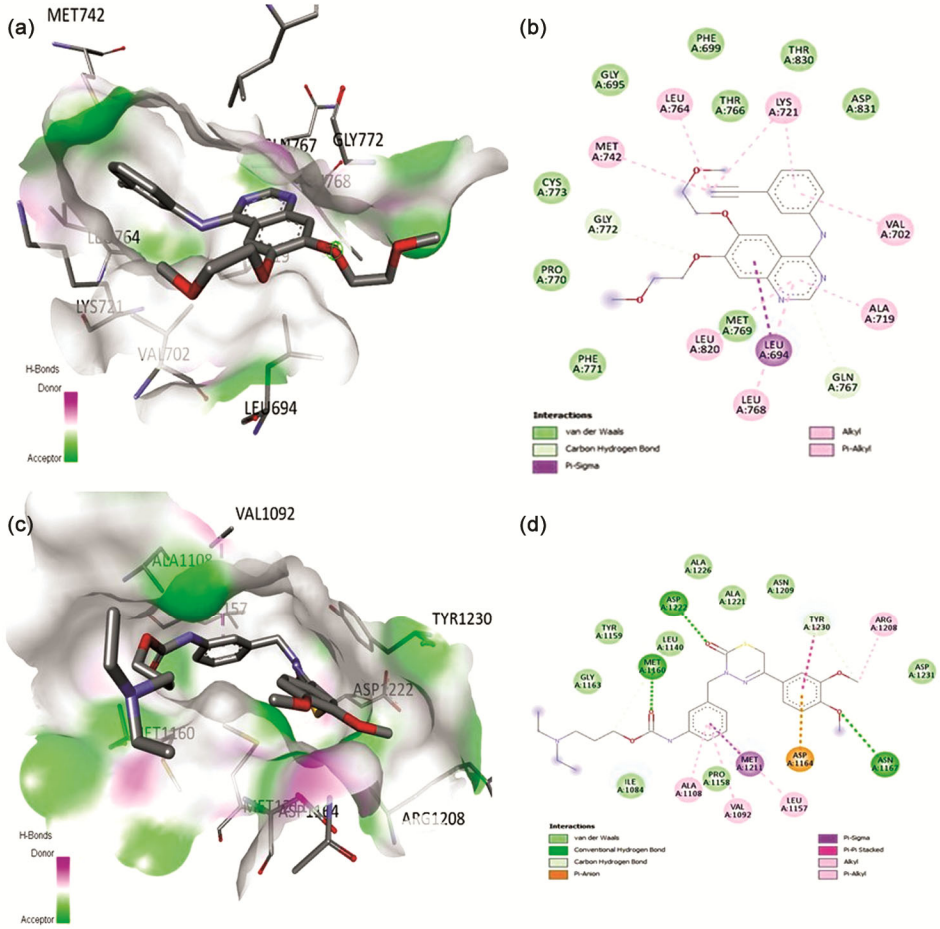

Fig. 2 — Amino acid interacting residues with 3D and 2D representation of co-crystallized ligands. A, B. Erlotinib with EGFR (PDB 1M17); C, D. Pyridazine derivative with MET (PDB 4R1Y). (*Contd*.)

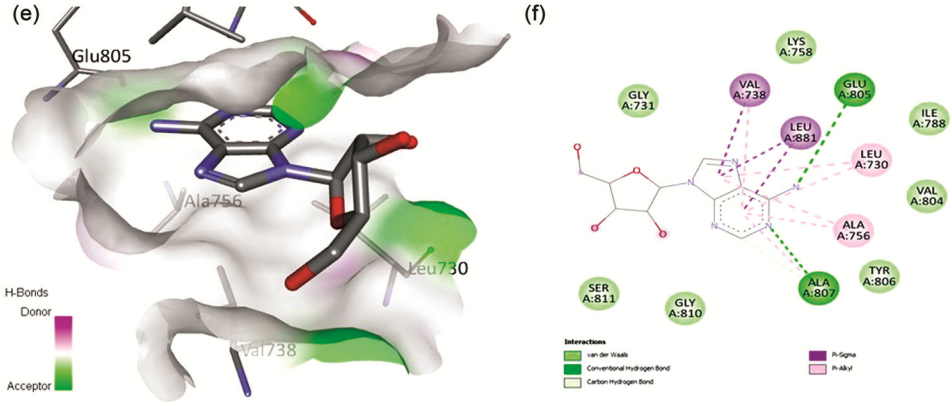

Fig. 2 — Amino acid interacting residues with 3D and 2D representation of co-crystallized ligands. E, F. Adenosine with RET (PDB 4CKJ).

Table 2 — 2D amino acid interaction of selected FDA approved antimalarial drugs with EGFR (PDB ID: 1M17), MET (PDB ID: 4R1Y), RET (PDB ID: 4CKJ)

Table 2A — 2D amino acid interaction of selected FDA approved antimalarial drugs with EGFR (PDB ID: 1M17)

Sr. No.	Drug	Amino acid interaction			2D interaction
		Hydrogen bonding interactions	Hydrophobic interactions	Miscellaneous	
1	Artesunate	THR830, LYS721	VAL702, LEU820, ALA719	-	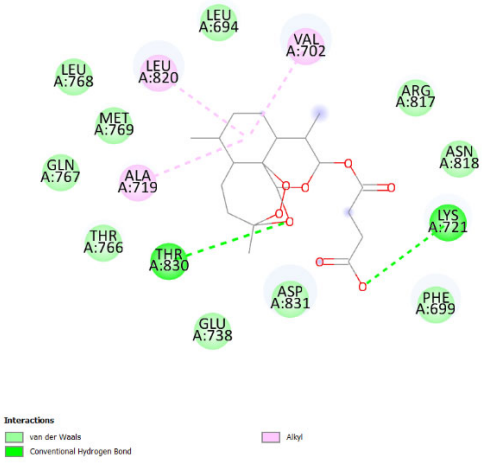
2	Atovaquone	THR830, ASP831, THR766	VAL702, LEU820, ALA719, LEU694, LEU764, LYS721	LYS721	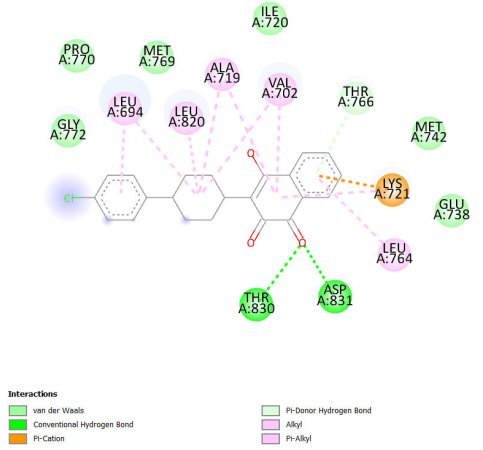

(*Contd.*)

Table 2 — 2D amino acid interaction of selected FDA approved antimalarial drugs with EGFR (PDB ID: 1M17), MET (PDB ID: 4R1Y), RET (PDB ID: 4CKJ) (*Contd.*)

Table 2A — 2D amino acid interaction of selected FDA approved antimalarial drugs with EGFR (PDB ID: 1M17)

Sr. No.	Drug	Amino acid interaction			2D interaction
		Hydrogen bonding interactions	Hydrophobic interactions	Miscellaneous	
3	Mefloquine	THR766, ALA719	PHE699, VAL702, LEU694, LEU820, LEU764, LYS721, MET742	ASP831	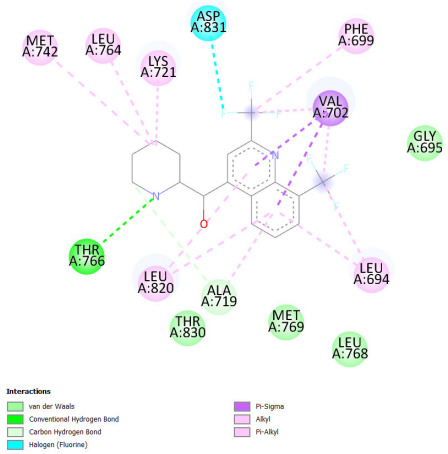
4	Quinine	THR766, ASP831	LEU820, ALA719, LEU694, VAL702, LYS721, ARG817, CYS773	-	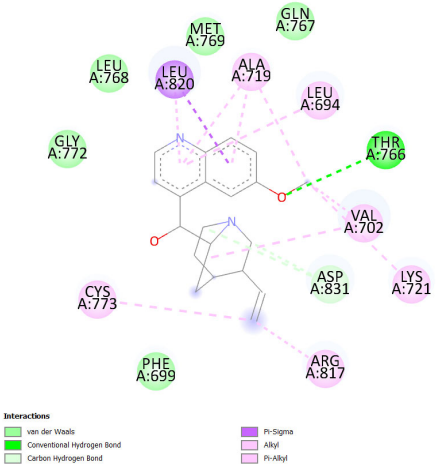

Table 2B — 2D amino acid interaction of selected FDA approved antimalarial drugs with MET (PDB ID: 4R1Y)

1	Artesunate	MET1160, TYR1159, GLY1085	TYR1230, MET1211, ALA1221	-	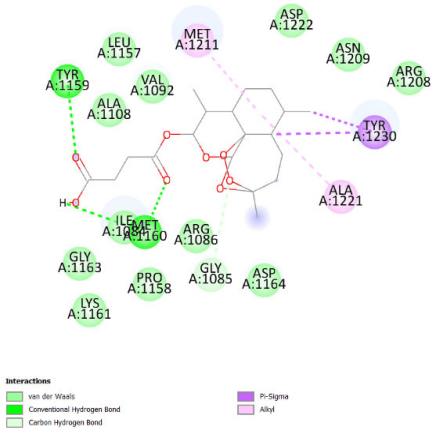

(*Contd.*)

Table 2 — 2D amino acid interaction of selected FDA approved antimalarial drugs with EGFR (PDB ID: 1M17), MET (PDB ID: 4R1Y), RET (PDB ID: 4CKJ) (*Contd.*)

Table 2B — 2D amino acid interaction of selected FDA approved antimalarial drugs with MET (PDB ID: 4R1Y)

Sr. No.	Drug	Amino acid interaction			2D interaction
		Hydrogen bonding interactions	Hydrophobic interactions	Miscellaneous	
2	Atovaquone	TYR1230, ASN1209	TYR1230, ALA1226, ALA1221, MET1211	MET1211	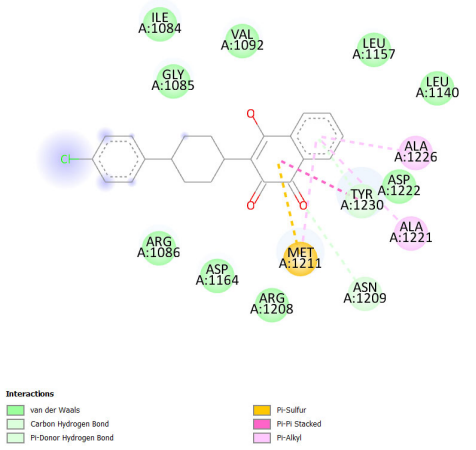
3	Mefloquine	ARG1086	TYR1230, MET1211, ALA1221, MET 1160, LEU1157, LEU1140, ALA1108, VAL1092	ASN1209, ARG1208, PRO1158	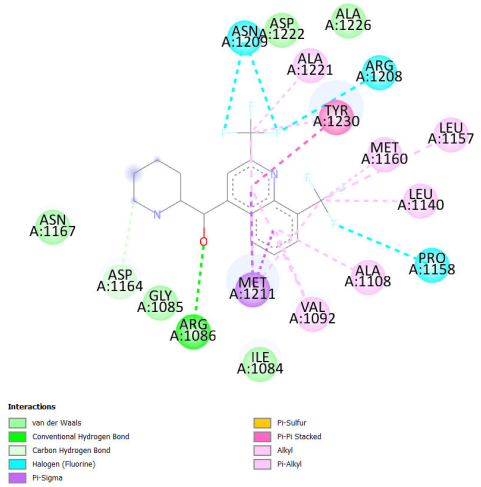
4	Quinine	TYR1230	TYR1230, MET1211, ALA1221, ALA1226, LEU1157, VAL1092, ALA1108	MET1211	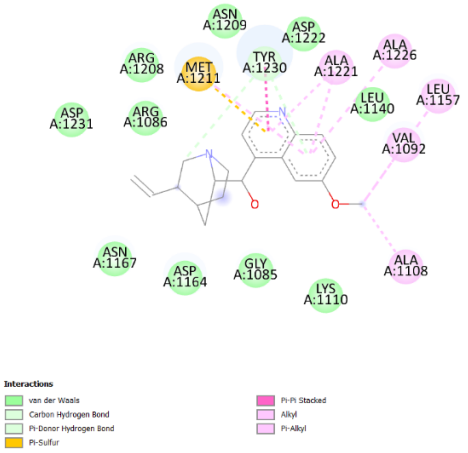

(*Contd.*)

Table 2 — 2D amino acid interaction of selected FDA approved antimalarial drugs with EGFR (PDB ID: 1M17), MET (PDB ID: 4R1Y), RET (PDB ID: 4CKJ)

Sr. No.	Drug	Amino acid interaction			2D interaction
		Hydrogen bonding interactions	Hydrophobic interactions	Miscellaneous	

Table 2C — 2D amino acid interaction of selected FDA approved antimalarial drugs with RET (PDB ID: 4CKJ)

1	Artesunate	SER811, GLY731	LEU730, LEU881	-	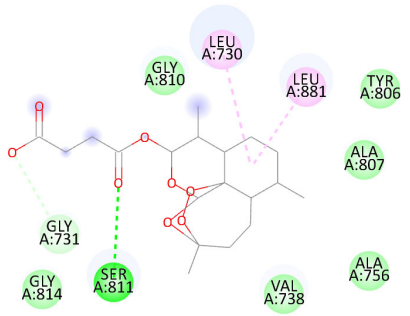
2	Atovaquone	LYS758	LEU730, LEU881, VAL738, ALA756, ALA807, ARG878	-	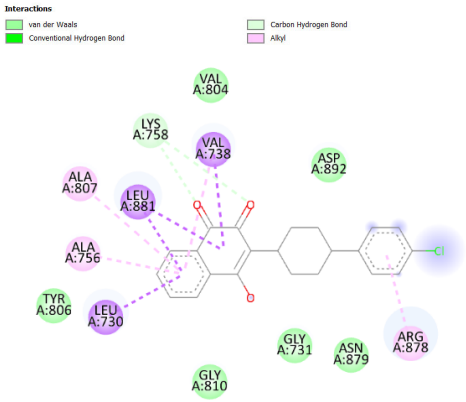
3	Mefloquine	ASP892, SER891	LYS758, LEU881, VAL738, VAL804, ALA756, TYR806, LEU730	LYS758, GLU805, ALA807	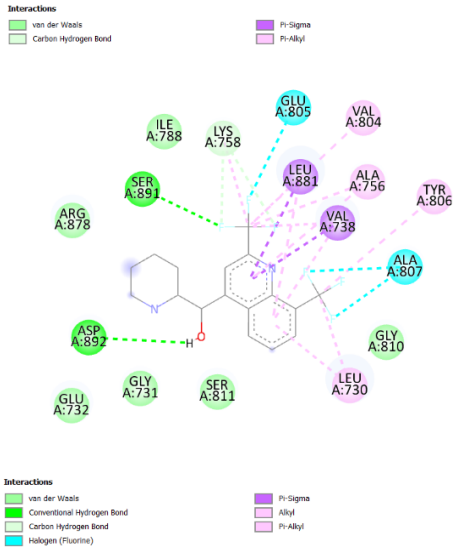

(*Contd.*)

Table 2 — 2D amino acid interaction of selected FDA approved antimalarial drugs with EGFR (PDB ID: 1M17), MET (PDB ID: 4R1Y), RET (PDB ID: 4CKJ)

Sr. No.	Drug	Amino acid interaction			2D interaction
		Hydrogen bonding interactions	Hydrophobic interactions	Miscellaneous	
Table 2C — 2D amino acid interaction of selected FDA approved antimalarial drugs with RET (PDB ID: 4CKJ)					
4	Quinine	SER891	LEU881, LEU730, ALA756, VAL738, ALA807		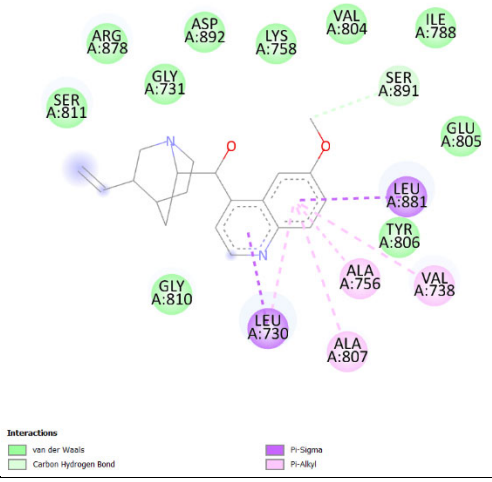

MQ, a quinoline analog widely used in combination with artemisinin for malaria treatment, works by inhibiting protein synthesis in *Plasmodium falciparum* through binding to the Pf80S ribosomal subunit[23]. Recent studies suggest that MQ also shows strong cytotoxicity and inhibits cell proliferation in various cancer types. *In vivo*, it has demonstrated effective tumor growth suppression, both as a standalone treatment and in combination with standard cancer therapies, enhancing their effects[24-26]. MQ's mechanisms of action include disrupting autophagy, interfering with lysosomal function, blocking key signaling pathways, and inhibiting P-glycoprotein pumps[27,28]. Given its proven anticancer efficacy in both lab and animal studies, along with its low cost and established clinical use, MQ holds significant promise as an adjunct or primary therapy in treating solid tumors and blood-related cancers.

Molecular interaction of MQ with EGRF

The crystal structure of the EGFR tyrosine kinase domain, exemplified by the PDB entry 1M17, reveals a bilobed architecture that is crucial for its functional role in cellular signaling. The N-lobe is characterized by a β-sheet and an alpha helix, which are instrumental in binding adenosine triphosphate (ATP) and ensuring its proper orientation during the activation of the kinase. This structural configuration is vital for the enzyme's activity, as it facilitates the precise positioning of ATP for subsequent phosphorylation reactions. In contrast, the C-lobe houses the catalytic and activation loop, both of which are essential for regulating kinase activity. The catalytic loop plays an important role in aligning ATP for the transfer of phosphate groups during signal transduction processes. Simultaneously, the activation loop undergoes conformational changes upon receptor activation, which enables downstream phosphorylation events that are crucial for propagating cellular signaling pathways[29,30]. Erlotinib, a prominent EGFR inhibitor, exerts its effects by binding to the ATP-binding region within the kinase domain of the receptor. This binding effectively obstructs ATP access, thereby preventing phosphorylation and halting EGFR-driven signaling pathways that may result in uncontrolled cell proliferation[31]. An interaction analysis of erlotinib with EGFR as shown in Fig. 2A illustrates several key interactions, including a C-H bond with GLN767, pi-sigma bonds with LEU694, and alkyl interactions with LYS721, MET742, and LEU764. Additionally, erlotinib forms pi-alkyl interactions with VAL702, ALA719, LEU768, and LEU820, further stabilizing its binding to the receptor. In comparison, mefloquine exhibits seven significant amino acid interactions with EGFR, paralleling those of erlotinib (Table 2A). Beyond these commonalities, mefloquine forms unique interactions that enhance its binding affinity and functional potential. Notably, it establishes a halogen bond with ASP831, an alkyl bond with

PHE699, and a hydrogen bond with THR766. These distinctive interactions suggest that mefloquine may target EGFR in a manner that contributes to its potential anticancer activity, indicating a promising avenue for further exploration in cancer therapeutics.

Molecular interaction of MQ with MET

The pyridazine derivative primarily targets the ATP-binding pocket of the MET receptor, located between its N-lobe and C-lobe[32]. Its binding is reinforced through various molecular interactions as shown in Fig. 2B, with key interactions including hydrogen bonds formed with critical residues such as ASN1167, MET1160, and ASP1222, ensuring a tight association with the receptor. In addition to these hydrogen bonds, hydrophobic interactions significantly contribute to the stability of the compound. These interactions encompass pi-pi bonding with TYR1230, which enhances the stability of the aromatic ring; pi-sigma bonding with MET1211, anchoring the pyridazine derivative more securely; and alkyl interactions with ARG1208, which promote non-polar stabilization of the molecule. Furthermore, pi-alkyl interactions with residues such as ALA1108, VAL1092, and LEU1157 augment van der Waals contacts, while pi-anion bonding with ASP1164 introduces an electrostatic component to the inhibitor's stability. C-H bonding with MET1160 and TYR1230 also plays a role, providing additional weak but significant stabilizing forces to maintain the inhibitor's position within the binding site. Collectively, these complex interactions enhance the inhibitory activity of the pyridazine derivative in the MET ATP-binding pocket. Similarly, the MQ shares eight common interactions with the pyridazine derivative (Table 2B), indicating its effectiveness in binding to the MET receptor as well. In addition to these shared interactions, MQ establishes unique bonds, such as a C-H bond with ARG1086, which adds further stability, and alkyl interactions with ALA1221, contributing to its hydrophobic stabilization. Furthermore, MQ forms a halogen bond with both ASN1209 and PRO1158, enhancing the drug's affinity for the MET receptor through specific halogen interactions that are critical for binding stability. These combined interactions illustrate the structural and functional complexity involved in the binding of both the pyridazine derivative and MQ to the MET receptor, emphasizing how they inhibit its function through multiple stabilizing forces.

Molecular interaction of MQ with RET

Adenosine is likely to bind to a specific region within the RET receptor, potentially at the interface between the two monomers or within the active site of the kinase domain[33]. Detailed interaction analysis reveals that adenosine forms key molecular interactions with the RET structure as shown in Fig. 2C. These include pi-sigma bonds with residues VAL738 and LEU881, and pi-alkyl interactions with ALA756 and LEU730, which help to stabilize the molecule within the binding pocket. In addition, hydrogen bonds are formed with critical residues GLU805 and ALA807, which further reinforce adenosine's binding affinity and stabilize its position in the RET receptor. MQ shares all the same interactions as adenosine, indicating a similar mode of binding (Table 2C). However, in MQ interactions with ALA807 and GLU805 involve halogen bonds rather than the hydrogen bonds observed with adenosine, due to the presence of halogen atoms in MQ's structure. These halogen bonds add an additional layer of stability to MQ's binding. Beyond these common interactions, MQ also forms unique bonds, including hydrogen bonds with ASP892 and SER891, enhancing its binding affinity. MQ further engages in alkyl interactions with LYS758, TYR806, and VAL804, contributing to its hydrophobic stabilization within the RET binding site. This combination of shared and unique interactions highlights MQ's strong binding to the RET receptor, reinforcing its inhibitory potential.

Further, MD simulations of MQ with EGFR, MET, and RET were conducted to investigate the stability and conformational dynamics of these drug-target complexes under physiological conditions. These simulations allowed for the observation of molecular interactions over time, offering insights into how MQ binds and stabilizes these critical NSCLC-related targets. Parameters such as RMSD, RMSF, and Rg were analyzed to assess the stability and flexibility of the complexes.

MD simulation of EGFR-MQ complex

For EGFR (PDB ID: 1M17), the RMSD analysis (Fig. 3A) demonstrated that both, erlotinib (inbuilt ligand, IN), and MQ achieved stability after 20 ns, maintaining consistent behavior throughout the simulation. The average RMSD values were 1.17 Å for the inbuilt ligand and 0.84 Å for MQ, indicating stable binding. RMSF analysis ((Fig. 3B), assessing

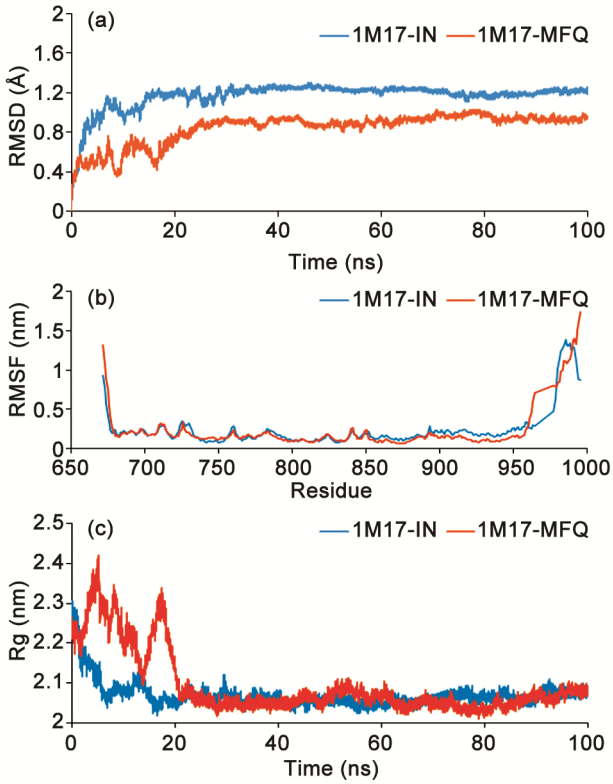

Fig. 3 — MD simulation of EGFR (PDB ID:1M17)-MQ complex A. RMSD; B. RMSF; and C. Rg

protein residue flexibility, showed reduced mobility at the binding site upon ligand binding, with average RMSF values of 0.23 Å and 0.22 Å for the IN and MQ, respectively. Additionally, a decreasing trend in Rg values (Fig. 3C) for both ligands suggested increased protein compactness, signifying structural stabilization induced by ligand binding. These findings confirm that MQ formed stable and robust interactions within EGFR's active site.

MD simulation of MET-MQ complex

For MET (PDB ID: 4R1Y), RMSD plots (Fig. 4A) demonstrated stabilization of all ligands after 10 ns, with average RMSD values of 0.22 Å and 0.32 Å for the pyridazinone derivative (inbuilt ligand, IN) and MQ, respectively. RMSF analysis (Fig. 4B) yielded comparable mean values for both ligands, while the Rg plots (Fig. 4C) suggested that mefloquine displayed a stability profile akin to the inbuilt ligand, highlighting its potential as a MET inhibitor.

MD simulation of RET-MQ complex

For RET (PDB ID: 4CKJ), RMSD plots (Fig. 5A) indicated that both adenosine (inbuilt ligand, IN) and

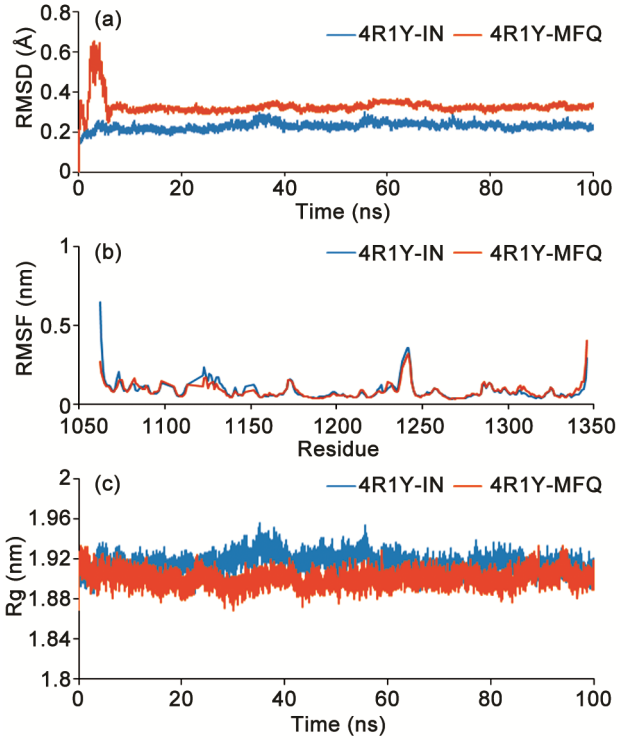

Fig. 4 — MD simulation of MET (PDB ID:4R1Y)-MQ complex A. RMSD; B. RMSF; and C. Rg

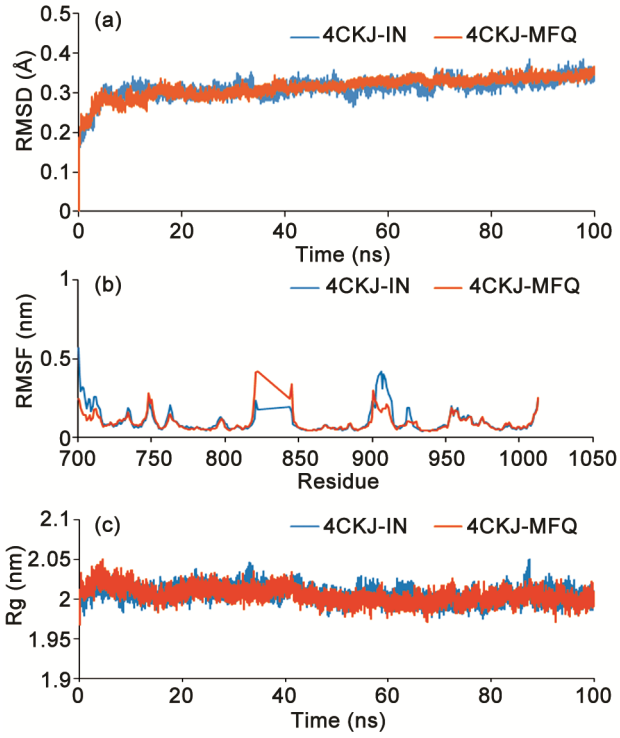

Fig. 5 — MD simulation of RET (PDB ID:4CKJ)-MQ complex A. RMSD; B. RMSF; and C. Rg

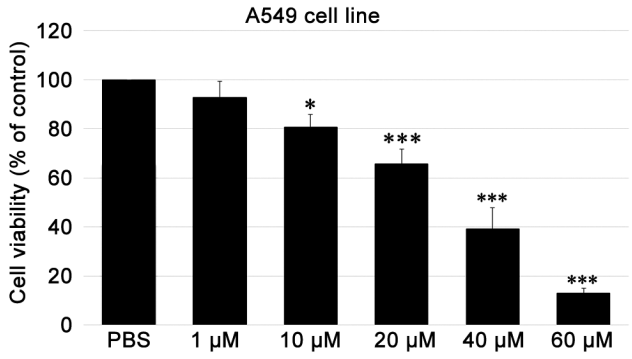

Fig. 6 — Inhibition of non small cell lung cancer cell (A549) proliferation by mefloquine *in vitro*. Relative cell viability (% of the PBS control) is presented as the mean ± standard error of the mean (SEM). Error bars represent the SEM (n=3). *P<0.05, ***P<0.001.

MQ reached stability after 10 ns, with similar RMSD values maintained until the end of the simulation. RMSF values averaged 0.10 Å for IN and 0.09 Å for MQ (Fig. 5B), reflecting consistent interactions. Rg plots (Fig. 5C) further confirmed comparable stabilization profiles for both ligands.

Biological evaluation

In this study, we investigated the effects of MQ on the proliferation of the A549 NSCLC cell line using the Sulforhodamine B (SRB) assay[22]. A549 cells were treated with increasing concentrations of MQ, and cell viability was assessed following a 48-hour of incubation period. The SRB assay, which quantifies cellular protein content as an indirect measure of cell density, was employed to assess the cytotoxic impact of MQ on the cancer cells. As illustrated in Fig. 6, MQ exhibited a dose-dependent inhibitory effect on A549 cell growth. The viability of the cells decreased progressively with increasing concentrations of the drug compared to the untreated control group. At a concentration as low as 10 µM, a significant reduction in cell viability was observed, highlighting the potency of MQ in suppressing the growth of NSCLC cells. This marked decrease suggests that MQ may disrupt essential cellular processes involved in cancer cell proliferation, making it a promising therapeutic candidate for further investigation in NSCLC treatment. Furthermore, the dose-dependent nature of this inhibition aligns with previous findings on MQ's activity against various cancer cell lines, suggesting that it may act through a conserved mechanism of cytotoxicity. These results warrant additional studies to elucidate the specific molecular pathways involved in MQ's anti-cancer effects and to explore its potential in combination with other therapeutic agents.

Conclusion

Lung cancer continues to be a major global health issue, with NSCLC making up the majority of cases. Despite advancements in treatment, current modalities face limitations such as drug resistance, significant side effects, and high costs. Repurposing FDA-approved drugs presents an innovative strategy to address these challenges, offering cost-effective and efficient therapeutic options. This study identified MQ as a promising candidate for NSCLC therapy, demonstrating superior binding affinity and stability with EGFR, MET, and RET proteins through molecular docking and dynamic simulations. MQ's dose-dependent cytotoxicity against A549 cells further supports its potential as an effective anti-NSCLC agent. Its established clinical use, low cost, and multi-targeted activity underscore its value in overcoming the limitations of current treatments. These findings highlight MQ as a potential standalone or adjunct therapy for NSCLC, paving the way for further research into its molecular mechanisms and combinatory therapeutic strategies to improve clinical outcomes.

Supplementary Information

Supplementary information is available on the website http://nopr.niscpr.res.in/handle/123456789/58776.

Acknowledgement

The authors wish to express their deep gratitude to Principal, Parul Institute of Pharmacy, Parul University, Vadodara, Gujarat, for providing the necessary facilities for carrying out the research work.

References

1 Zhou J, Xu Y, Liu J, Feng L, Yu J & Chen D, *Cancer Epidemiol*, 93(2024) 102693.
2 Gridelli C, Rossi A, Carbone D P, Guarize J, Karachaliou N, Mok T, Petrella F, Spaggiari L & Rosell R, *Nat Rev Dis Primers*, 1 (2015) 1.
3 Jones G C, Kehrer J D, Kahn J, Koneru B N, Narayan R, Thomas T O, Camphausen K, Mehta M P & Kaushal A, *Clin Lung Cancer*, 16 (2015) 413.
4 Kumar A & Kumar A, *Adv Cancer Biol - Metastasis*, 6 (2022) 100076.
5 Rebuzzi S E, Zullo L, Rossi G, Grassi M, Murianni V, Tagliamento M, Prelaj A, Coco S, Longo L, Dal Bello M G & Alama A, *Int J Mol Sci*, 22 (2021) 2625.
6 Zubair T & Bandyopadhyay D, *Int J Mol Sci*, 24 (2023) 2651.

7 Santarpia M, Massafra M, Gebbia, V, D'Aquino A, Garipoli C, Altavilla G & Rosell R, *Transl Lung Cancer Res*, 10 (2021) 1536.
8 Desilets A, Repetto M, Yang S R, Sherman E J & Drilon A, *Cancers*, 15 (2023) 4146.
9 Pant J, Mittal P, Singh L & Marwah H, *Curr. Pharmacogenomics Pers Med*, 20 (2023) 146-164.
10 Hua Y, Dai X, Xu Y, Xing G, Liu H, Lu T, Chen Y & Zhang Y, *Eur J Med Chem*, 234 (2022) 114239.
11 Wuerth R, Thellung S, Bajetto A, Mazzanti M, Florio T & Barbieri F, *Drug Disc Today*, 21 (2016) 190.
12 Hijazi M A, Gessner A & El-Najjar N, *Cancers*, 15 (2023) 3199.
13 Famurewa A C, Mukherjee A G, Wanjari U R, Sukumar A, Murali R, Renu K, Vellingiri B, Dey A & Gopalakrishnan A V, *Life Sci*, 305 (2022) 120789.
14 Mohi-Ud-Din R, Chawla A, Sharma P, Mir P A, Potoo F H, Reiner Ž, Reiner I, Ateşşahin, D A, Sharifi-Rad J, Mir R H & Calina D, *Eur J Med Res*, 28 (2023) 345.
15 Salentin S, Adasme M F, Heinrich J C, Haupt V J, Daminelli S, Zhang & Schroeder M, *Sci Rep*, 7 (2017) 11401.
16 Dai X, Zhang X, Chen W, Chen Y, Zhang Q, Mo S & Lu J, *Int J Biol Sci*, 17 (2021) 603.
17 Ovejero-Sánchez M, Gonzalez-Sarmiento R & Herrero A B, *Neoplasia*, 23 (2021) 515.
18 Kitchen DB, Decornez H, Furr J R & Bajorath J, *Nat Rev Drug Disc*, 3 (2004) 935.
19 Warren G L, Andrews C W, Capelli A M, Clarke B, LaLonde J, Lambert M H, Lindvall M, Nevins N, Semus S F, Senger S & Tedesco G, *J Med Chem*, 49 (2006) 5912.
20 Wong W, Bai X C, Sleebs B E, Triglia T, Brown A, Thompson J K, Jackson K E, Hanssen E, Marapana D S, Fernandez I S & Ralph S A, *Nat Microbio*, 2 (2017) 1.
21 Yan K H, Lin Y W, Hsiao C H, Wen Y C, Lin K H, Liu C C, Hsieh M C, Yao C J, Yan M D, Lai G M & Chuang S E, *Oncol Lett*, 5 (2013) 1567.
22 Xu X, Wang J, Han K, Li S, Xu F & Yang Y, *Cancer Sci*, 109 (2018) 1220.
23 Tao Q, Liu N, Wu J, Chen J, Chen X & Peng C, *J Imm Ther Can*, 12 (2024).
24 Ghosh D K, Kumar A & Ranjan A, *Toxicology*, 464 (2021) 152995.
25 Mereddy G & Ronayne C J, *Transl Med*, 8 (2018) 2161.
26 Hubbard S R, *Prog Biophy Mol Biol*, 71 (1999) 343.
27 Nie W, Tang L, Zhang H, Shao J, Wang Y, Chen L, Li D & Guan X, *Int J Oncol*, 40 (2012) 1763.
28 Park J H, Liu Y, Lemmon M A & Radhakrishnan R, *Biochem J*, 448 (2012) 417.
29 Kim K S, Zhang L, Schmidt R, Cai Z W, Wei D, Williams DK, Lombardo L J, Trainor G L, Xie D, Zhang Y & An Y, *J Med Chem*, 51 (2008) 5330.
30 Plaza-Menacho I, Barnouin K, Goodman K, Martínez-Torres R J, Borg A, Murray-Rust J, Mouilleron S, Knowles P & McDonald N Q, *Mol Cell*, 53 (2014) 738.
31 Orellana E A & Kasinski A L, *Bio-protoc*, 6 (2016) 1984.
32 Morris G M, Huey R, Lindstrom W & Sanner M F, *J Comp Chem*, 19 (2009) 2785.
33 Schmid N, Eichenberger A P, Choutko A, Riniker S, Winger M, Mark A E & Van Gunsteren W F, *Eur Biophys J*, 40 (2011) 843.